JOURNAL OF COORDINATION CHEMISTRY
2021, VOL. 74, NOS. 9–10, 1366–1381
https://doi.org/10.1080/00958972.2021.1914332

4,5-Diazafluorene ligands and their ruthenium(II) complexes with boronic acid and catechol anchoring groups: design, synthesis and dye-sensitized solar cell applications

Caner Cebeci[a], Barış Seçkin Arslan[b], Emre Güzel[c], Mehmet Nebioğlu[b,d], İlkay Şişman[b,d] and İbrahim Erden[a]

[a]Department of Chemistry, Yıldız Technical University, Istanbul, Turkey; [b]Department of Chemistry, Sakarya University, Sakarya, Turkey; [c]Department of Fundamental Sciences, Sakarya University of Applied Sciences, Sakarya, Turkey; [d]Department of Renewable Energy Systems, Sakarya University, Sakarya, Turkey

ABSTRACT

Design, synthesis, characterization, and investigation of photovoltaic properties of 4,5-diazafluorene derived diimine ligands (**C2**, **C3**) and their ruthenium(II) complexes are reported. FT-IR, ^{1}H NMR, ^{13}C NMR, and mass spectroscopic methods were used to elucidate the structures of these compounds. The effect of the number and nature of anchoring groups attached to these ligands and complexes as sensitizers were evaluated for optical properties and photovoltaic performance in dye-sensitized solar cells (DSSCs). The sensitizers bearing catechol show higher power conversion efficiency (PCE) than the dyes with boronic acid due to better binding of the catechol anchoring group on the TiO_2 surface. Among these sensitizers, DSSC based on **[Ru(C2)$_2$(NCS)$_2$](PF$_6$)$_2$** having two catechol anchoring groups gives the best PCE of 2.83%, with $J_{sc} = 6.40\,mA\,cm^{-2}$, $V_{oc} = 0.632\,V$ and $FF = 0.70$ in the presence of chenodeoxycholic acid (CDCA) as the coadsorbent, which is attributed to broader spectral response and efficient electron injection. These results suggest that dyes bearing two catechol anchoring groups are promising for efficient DSSCs.

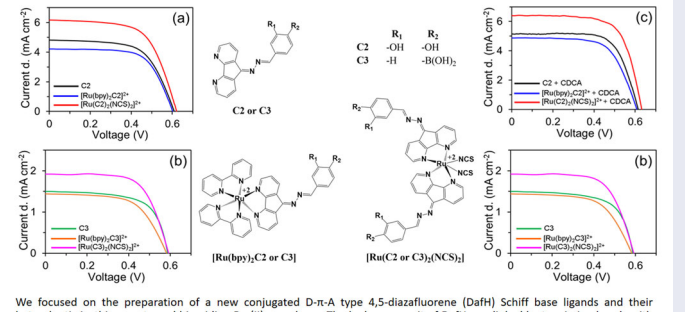

We focused on the preparation of a new conjugated D-π-A type 4,5-diazafluorene (DafH) Schiff base ligands and their heteroleptic isothiocyanate and bipyridine Ru (II) complexes. The hydrazone unit of DafH was linked by two imine bonds with the phenylboronic acid and catechol moieties. DafHs and their heteroleptic Ru (II) complexes were evaluated for DSSCs performance by comparison with both each other and N719 standard dye. While dyes with boronic acid moiety didn't exceed, catechol moiety exceeded 2% PCE.

ARTICLE HISTORY

Received 10 November 2020
Accepted 19 March 2021

KEYWORDS

4,5-Diazafluorene; ruthenium(II) complexes; photosensitizer; photovoltaic; dye-sensitized solar cells

CONTACT Barış Seçkin Arslan Barisseckin@Gmail.com Department of Chemistry, Sakarya University, Sakarya, Turkey; İbrahim Erden ierden@Yildiz.edu.tr Department of Chemistry, Yıldız Technical University, Istanbul, Turkey

Supplemental data for this article is available online at https://doi.org/10.1080/00958972.2021.1914332.

1. Introduction

Globally, the excessive use of fossil fuels to meet increasing energy demand brings both environmental and health issues. As an alternative, harvesting energy from sunlight with photovoltaics is essential for future global energy production. Dye-sensitized solar cells (DSSCs) which were pioneered by Gratzel and O'Regan appeal to widespread scientific research and technological interest as solar cell candidates [1].

Device architecture of DSSCs consists of transparent conductive oxide glass substrate, wide-band-gap semiconductor (by a majority TiO_2), sensitizer, a redox electrolyte solution, and a counter electrode. Effective electron injection between the dye and TiO_2 nanoparticle interface is crucial for improving the power conversion efficiency (PCE) of DSSCs. Another crucial point is preventing energy losses in electron injection [2]. To improve solar energy conversion efficiency of DSSCs, modifications of TiO_2 photoanode [3], synthesizing new dye molecules as sensitizers [4, 5], developing new electrolytes [6] and anchoring groups [7] play substantial roles for future use of such devices.

4,5-Diazafluorene (dafH), which was first reported by Kloc and colleagues is a heterocyclic compound with two nitrogen donors for metal coordination like 1,10-phenanthroline and bipyridine [8]. DafHs are synthesized from oxidative ring contraction reaction of 1,10-phenanthroline with potassium permanganate in basic aqueous media [9]. DafH derivatives have been studied in biological activities [10–12], non-halogen flame retardants [13], OFET [14], catalysts [15, 16], polyurethane curing agents [17], sensors [18–21], high-performance polyimide [22] and OLEDs [23, 24]. DafHs have shown various solar cell performances between 0.22% and 3.45% in their DSSC applications [25–32].

Carboxylic acid anchoring group containing sensitizers were widely used for DSSCs owing to their sufficient binding to TiO_2 surface in organic solvents. However, there are two disadvantages of carboxylic acids including very low pKa values to provide strong binding on TiO_2 and its propensity to detach from the TiO_2 surface in the presence of water. These two handicaps limit the long-term stability of cells [33, 34]. Because of these disadvantages, alternative anchoring groups need to be investigated for long-term use of DSSCs. The binding properties of the complexes bearing catechol anchoring groups to TiO_2 surface are superior to the complexes bearing carboxylic acid due to a five-membered ring formed between Ti^{4+} and the catechol moiety [35]. Although previous studies of catechol anchoring groups have not exceeded 2% PCE, this has been transcended with 4.87. However, a disadvantage is the ZnPTC-coded compound has a long synthesis procedure [34]. As a search for different anchoring groups, boronic acids are considered promising and an alternative to carboxylic acid anchors [36]. Dyes bearing boronic acid have two monodentate or four bridging bidentate anchoring modes on TiO_2 [37]. However, there are only a few studies about organic-inorganic hybrid solar cell applications involving boronic acid anchors [38–40].

Among natural, organic and inorganic sensitizers, ruthenium complexes have been investigated as sensitizers due to their stability and superior redox properties [41]. Both for improving deficiencies and adding new approaches, herein, we focus on preparation of conjugated D-π-A type Schiff base ligands and their heteroleptic Ru(II) complexes of dafH compounds. Hydrazone unit of dafH was linked with aldehyde

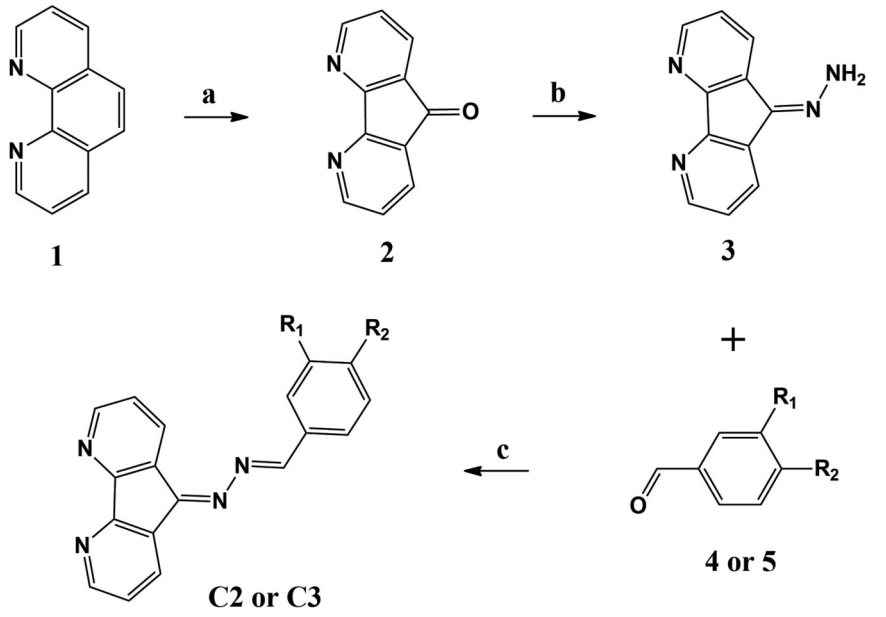

Ligands	R_1	R_2	Starting Compounds
C2	-OH	-OH	4
C3	-H	$-B(OH)_2$	5

Scheme 1. The synthesis of 4,5-diazafluorene ligands: (a) $KMnO_4$, KOH, H_2O, Δ; (b) AcOH, NH_2NH_2, MeOH, 8 h; (c) toluene, 16 h, p-toluenesulfonic acid, 105–115 °C.

units of 3,4-dihydroxybenzaldehyde and 4-formylphenylboronic acid by imine bond formation (Scheme 1). Both isothiocyanate and bipyridine heteroleptic Ru(II) complexes of dafH ligands were prepared to make PCE comparisons between the ligands and their Ru complexes. The synthesized compounds were characterized by FT-IR, UV-Vis, ^{1}H NMR, ^{13}C NMR, and mass spectroscopic methods.

2. Materials and methods

2.1. Instruments and chemicals

The aldehyde compounds, 3,4-dihydroxybenzaldehyde (**4**) and 4-formylphenylboronic acid (**5**), were purchased from Aldrich and used as received. All chemicals were supplied as reagent grade from Fluka and Merck. FT-IR spectra were recorded on a Nicolet iS10 spectrometer using attenuated total reflection (ATR). NMR spectra were recorded on a Bruker Avance III 500 MHz spectrometer in methanol-d_4 and DMSO-d_6 using tetramethylsilane (TMS) as an internal standard. Absorption spectra were recorded with a Shimadzu-2600 UV spectrometer. Mass spectra of dafHs were recorded on Agilent 6530/Agilent HPLC LCMS QTOF. Mass spectra of ruthenium complexes were recorded on Bruker Microflex LT MALDI-TOF MS in Gebze Technical University.

2.2. Synthesis

The starting compounds 4,5-diazafluorene-9-one (**2**), 4,5-diazafluorene-9-hydrazone (**3**), *cis*-$(bpy)_2RuCl_2{\cdot}2H_2O$ were synthesized and purified according to literature procedures [8, 42–44]. FT-IR spectra of **2**–**5** are given in the Supplementary Information (Figures S1–S4).

2.3. Synthesis of the compounds

2.3.1. Synthesis of 4-(((5H-cyclopenta[1,2-b:5,4-b′]dipyridin-5-ylidene)hydrazono)-methyl)benzene-1,2-diol (C2)

4,5-Diazafluorene-9-hydrazone (93 mg, 0.474 mmol), 3,4-dihydroxybenzaldehyde (68.7 mg, 0.498 mmol), catalytic amount of p-toluenesulfonic acid and 25 mL toluene were added to a 50 mL single-neck, round-bottom flask and stirred at 105–115 °C under argon for 14 h. Progress of the reaction was monitored by TLC on silica with chloroform/methanol (4:1) as eluent. After the solvent was halved by rotary evaporation, the crude product was precipitated at room temperature, filtered with D4 filter crucible borosilicate glass, washed with 10 mL cold diethyl ether and 10 mL cold water twice for purification and dried in vacuum overnight at 40 °C. 120 mg red solid product was obtained. Yield: 80%. m.p.: 232 °C. FT-IR (cm^{-1}): 3551 and 3495 ν(O-H), 3200–2800 ν(broad, O-H), 1624 ν(9-position of dafH, C = N), 1613 and 1598 (C = N dafH), 1583 and 1542, ν(Ph, C = C). ^{1}H NMR (500 MHz, MeOD) δ 9.14 (s, 2H), 8.78 (s, 1H), 8.63 (d, J = 13.7 Hz, 1H), 8.50 (s, 2H), 7.70 (d, J = 17.5 Hz, 1H), 7.57 (s, 1H), 7.45–7.09 (m, 3H), 6.87 (dd, J = 62.5, 31.8 Hz, 2H). LCMS-QTOF: *m/z*: 317.10 ($M + H^+$).

2.3.2. Synthesis of (4-(((5H-cyclopenta[1,2-b:5,4-b′] dipyridin-5-ylidene)hydrazono)-methyl)phenyl) boronic acid (C3)

Same synthesis procedure with synthesis of **C2** was applied for synthesis of **C3** with the following amounts of starting compounds: 4,5-diazafluorene-9-hydrazone (119.59 mg, 0.61 mmol) and 4-formylphenylboronic acid (96 mg, 0.64 mmol). 170 mg yellow solid product was obtained. Yield: 85%. m.p.: 257 °C. FT-IR (cm^{-1}): 3400–2700 ν(broad, O-H), 1628 ν(9-position of dafH, C = N), 1599 (C = N dafH), 1572 and 1536 ν(Ph, C = C). ^{1}H NMR (500 MHz, DMSO) δ 8.82 (d, J = 15.5 Hz, 1H), 8.78 (s, 1H), 8.72 (s, 1H), 8.31 (s, 1H), 8.00 (d, J = 11.7 Hz, 2H), 7.93–7.82 (m, 2H), 7.57 (d, J = 19.1 Hz, 1H), 7.47 (d, J = 7.7 Hz, 2H), 7.12 (d, J = 7.6 Hz, 2H). LCMS-QTOF: *m/z*: 329.11 ($M + H^+$).

2.3.3. Synthesis of $[Ru(bpy)_2C2](PF_6)_2$

cis-$(bpy)_2RuCl_2$ (59 mg, 0.122 mmol), **C2** (39 mg, 0.123 mmol), KPF_6 (45.12 mg, 0.27 mmol) and 15 mL methanol were added to a 25 mL single-neck, round-bottom flask and stirred at 60–65 °C under argon for 12 h. After the solvent was removed by rotary evaporation, the crude product was washed with 10 mL cold methanol and 10 mL cold water twice for removing excess **C2** and KPF_6 and dried in vacuum overnight at 40 °C. 65 mg red solid product was obtained. Yield: 52%. FT-IR (cm^{-1}): 3087 ν(Ph, C = H), 1628 ν(9-position of dafH, C = N), 1603, 1590, 1463, 1446, 833. MALDI-TOF: *m/z* 730.725 and 875.457 ($M + PF_6^+$).

2.3.4. Synthesis of $[Ru(bpy)_2C3](PF6)_2$

The same synthesis procedure as for $[Ru(bpy)_2C2](PF_6)_2$ was applied for synthesis of $[Ru(bpy)_2$**C3**$](PF_6)_2$ with the following amounts of starting compounds: *cis*-$(bpy)_2RuCl_2$ (58 mg, 0.12 mmol), **C3** (39 mg, 0.122 mmol), KPF_6 (45 mg, 0.24 mmol). 47 mg red solid product was obtained. Yield: 37.6%. FT-IR (cm^{-1}): 3085 ν(Ph, C = H), 1628 ν(9-position of dafH, C = N), 1604, 1536, 1464, 1446, 831. MALDI-TOF: *m/z* 741.723, 886.947 (M + PF_6+), 1063.830 (M + 2PF6 + MeOH) and 1209.174 (M + 3PF6 + MeOH).

2.3.5. Synthesis of $[Ru(C2)_2(NCS)_2](PF_6)_2$

$RuCl_3{\cdot}H_2O$ (22.75 mg, 0.11 mmol), **C2** (69.38 mg, 0.22 mmol), a small amount of LiCl and 12 mL DMF were added to a 25 mL single-neck, round-bottom flask and stirred at 150–160 °C under argon for 8 h. After the color of the reaction mixture turned violet, NH_4NCS (17 mg, 0.223 mmol), KPF_6 (42 mg, 0.228 mmol) and 3 mL DMF were added to the reaction flask and the reaction was continued for 12 h under an argon atmosphere at 150–160 °C. The solvent was removed by rotary evaporation, crude product was washed with 10 mL cold methanol and 10 mL cold water twice for removing excess **C2**, NH_4NCS and KPF_6 and dried in vacuum overnight at 40 °C. 72 mg black solid product was obtained. Yield: 57.6%. FT-IR (cm^{-1}): 3400–2600 ν(broad, O-H), 3077 ν (Ph, C = H), 2103 and 1966 (-NCS), 1726 ν (9-position of dafH, C = N), 1656 and 1594 ν (C = N dafH), 1413, 1286, 806, 739. MALDI-TOF: *m/z* 851(M+).

2.3.6. Synthesis of $[Ru(C3)_2(NCS)_2](PF_6)_2$

The same synthetic procedure as for $[Ru($**C2**$)_2(NCS)_2](PF_6)_2$ was applied for synthesis of $[Ru($**C3**$)_2(NCS)_2](PF_6)_2$ with the following amounts of starting compounds: $RuCl_3{\cdot}H_2O$ (22.3 mg, 0.107 mmol), **C2** (70.51 mg, 0.214 mmol), a small amount of LiCl, NH_4NCS (16.50 mg, 0.215 mmol), KPF_6 (40 mg, 0.217 mmol). FT-IR (cm^{-1}): 3800–2500 ν (broad, O-H), 3078 ν (Ph, C = H), 2103 and 1965 (-NCS), 1722ν (9-position of dafH, C = N), 1626 and 1595 ν (C = N dafH), 1434, 1285, 807, 738. MALDI-TOF: *m/z* 992.5 (M + 4MeOH+), 963.6 (M + 3MeOH+) 941.4 (M + MeOH+).

3. Results and discussion

3.1. Synthesis and characterization

For the synthesis of **C2** and **C3**, three-step synthetic processes were performed. First, **2** was obtained from **1** via oxidative ring contraction with potassium permanganate in basic aqueous media. Second, **3** was obtained via the reaction of **2** with hydrazine hydrate in acidic medium. In the last step, the condensation reaction of **4** with **3** resulted in **C2** formation and the condensation of **5** with **3** resulted in **C3** formation. Because Schiff base (**C2**, **C3**) formation is a reversible reaction, the reactions were carried out both in the presence of p-toluenesulfonic acid as a catalyst and at a temperature above 100 °C to remove water from the reaction medium.

Formation of **C2** and **C3** were shown with disappearance of the primary amine stretching bands of **3** at 3368 and 3310 cm^{-1}, the disappearance of the carbonyl stretching band of related aldehydes, respectively, at 1644 (**4**), 1663 cm^{-1} (**5**) and occurrence of azomethine stretches of resulting compounds at 1624 (**C2**) and

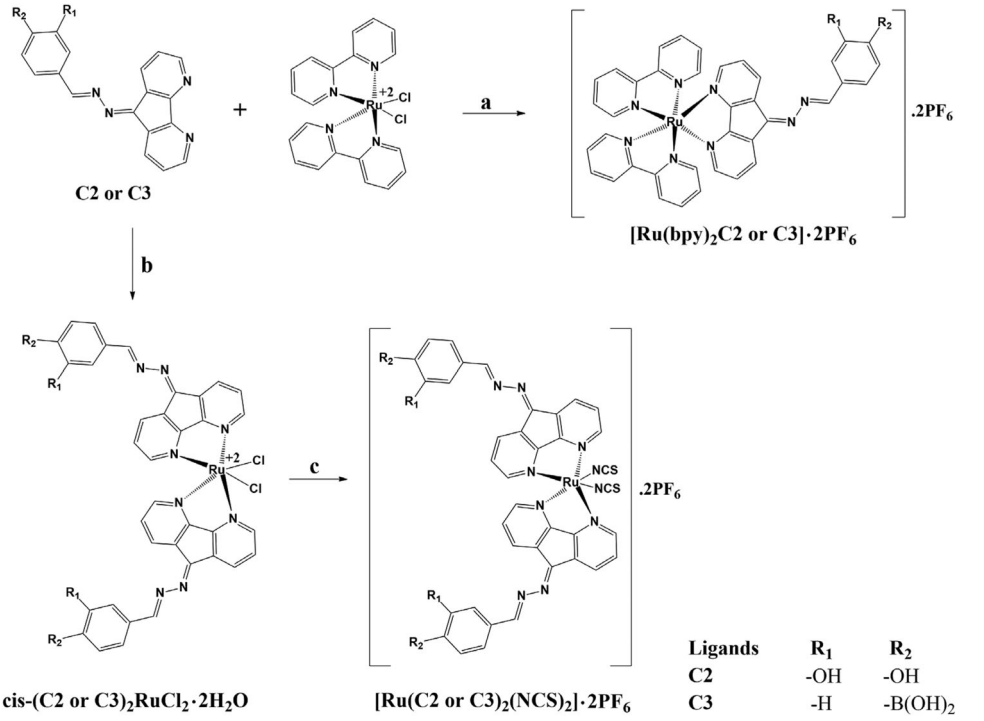

Scheme 2. The synthesis of heteroleptic ruthenium complexes of 4,5-diazafluorene ligands: (a) MeOH, 60–65 °C, 12 h; (b) $RuCl_3{\cdot}H_2O$, LiCl, DMF, 150–160 °C, 8 h; (c) NH_4NCS, KPF_6, DMF, 150–160 °C, 12 h.

1628 cm^{-1} (**C3**) in their infrared spectra (Supplementary Information Figures S3–S5 and S8). ^1H NMR spectra of **C2** and **C3** are given in the Supplementary Information (respectively Figures S6 and S9) and recorded in methanol-d_4 (**C2**) and DMSO-d_6 (**C3**). ^{13}C NMR spectra of **C2** and **C3** were not recorded due to insufficient solubility of the compounds in deuterated solvents. The molecular ion peaks of **C2** and **C3** appeared at *m/z*: 317.10 (M + H+) and *m/z*: 329.11 (M + H+), respectively.

Ruthenium bipyridine complexes of **C2** and **C3** were synthesized with 1:1 molar ratio of ligand/*cis*-$(bpy)_2RuCl_2{\cdot}2H_2O$. Ruthenium isothiocyanate complexes of **C2** and **C3** were synthesized with one-pot, two-step synthetic processes. First, *cis*-(**C2** or **C3**)$_2RuCl_2{\cdot}2H_2O$ complexes of ligands were synthesized. When the reaction mixture turned violet after 8 h, NH_4NCS and KPF_6 were added to the mixture and the reaction was continued another 12 h until it turned black. LiCl was used to prevent dissociation of Cl^- in the synthesis of *cis*-(**C2** or **C3**)$_2RuCl_2{\cdot}2H_2O$ complex [45]. KPF_6 was used as a counter ion source (PF_6^-) in all complexes (Scheme 2).

In FT-IR spectra of the ruthenium bipyridine complexes of **C2** and **C3**, the transmittance of the $C=N_{fluorene}$ stretching bands decreased and 1750–4000 cm^{-1} region flattened when compared with related FT-IR spectrum of **C2** and **C3**. These results suggest that coordination occurred. Determination of the molecular mass of complexes with the MALDI-TOF technique is useful to prove the synthesis. Dithranol (**DIT**) for **[Ru(bpy)$_2$C2](PF$_6$)$_2$** and 2,5-dihydroxybenzoic acid (**DHB**) for **[Ru(bpy)$_2$C3](PF$_6$)$_2$**

were used as a matrix for molecular mass determination of **[Ru(bpy)$_2$C2](PF$_6$)$_2$** and **[Ru(bpy)$_2$C3](PF$_6$)$_2$** complexes with MALDI-TOF. Molecular ion peaks of **[Ru(bpy)$_2$C2]** [*m/z*: 730.725, 875.457 ($M + PF_6^+$)] and **[Ru(bpy)$_2$C3](PF$_6$)$_2$** [*m/z*: 886.947 ($M + PF_6^+$), 1063.830 ($M + 2PF_6$+MeOH), 1209.174 ($M + 3PF_6$+MeOH)] proved formation of complexes. Apart from **[Ru(bpy)$_2$C2](PF$_6$)$_2$**, methanol (MeOH) molecules were also observed in the mass spectrum of **[Ru(bpy)$_2$C3](PF$_6$)$_2$** due to keeping MeOH in its structure. While dissolving the compound in MeOH for the target plate of MALDI-TOF in sample preparation, the occurrence of molecular interactions between boronic acid with MeOH is considered the reason for keeping MeOH in the structure of **C3**.

In the characterization of ruthenium isothiocyanate complexes of **C2** and **C3**, two peaks in FT-IR spectra at 2102 and 1965–1966 cm^{-1} indicate that isothiocyanate ligands are *cis* [44]. ν(C = S) stretch at 739 cm^{-1} (**C2**) and 738 cm^{-1} (**C3**) also showed N-coordination of the isothiocyanate group with ruthenium. Molecular mass of ruthenium isothiocyanate complexes of **C2** and **C3** were determined with the MALDI-TOF technique similarly with ruthenium bipyridine complexes. While *trans*-2-[3-(4-tert-butylphenyl)-2-methyl-2-propenylidene]malononitrile (**DCTB**) was used as a MALDI-TOF matrix for determining the mass of **[Ru(C2)$_2$(NCS)$_2$](PF$_6$)$_2$**, no matrix was used for **[Ru(C3)$_2$(NCS)$_2$](PF$_6$)$_2$**. Formation of complexes were understood with molecular ion peaks of **[Ru(C2)$_2$(NCS)$_2$]$^{2+}$** [*m/z* 851(M^+)] and **[Ru(C3)$_2$(NCS)$_2$]$^{2+}$** [*m/z* 992.5 ($M + 4MeOH^+$), 963.6 ($M + 3MeOH^+$) 941.4 ($M + MeOH^+$)]. Similarly, with **[Ru(bpy)$_2$C3]$^{2+}$**, MeOH molecules were also observed in the mass of **[Ru(C3)$_2$(NCS)$_2$]$^{2+}$** complex due to dissolving ruthenium isothiocyanate complexes in MeOH/DMF solvent mixture in sample preparation for target plate of MALDI-TOF.

3.2. Optical properties

UV-Vis absorption spectra of **C2** and **C3** and their ruthenium complexes in methanol are shown in Figure 1. The optical properties of all compounds are given in Table 1. Absorptions at 228, 316 and 388 nm were assigned to π-π* transition of **C2** and absorptions at 229, 316 and 337 nm for **C3** [46]. **C2** which has catechol moiety exhibited red-shifted absorption (388 nm) while **C3** having boronic acid group (337 nm) may be due to the resonance and electron-donating ability of phenolic -OH groups. Intraligand π-π* transitions were seen at 210–287 nm for $[Ru(bpy)_2C2]^{2+}$ and 208–287 nm for $[Ru(bpy)_2C3]^{2+}$. Characteristic metal-to-ligand charge-transfer (MLCT) transitions for **[Ru(bpy)$_2$C2]$^{2+}$** and **[Ru(bpy)$_2$C3]$^{2+}$** were observed at 442 and 423 nm, respectively. Absorption bands at 227, 316, 386 nm and 214, 315, 353 nm were assigned to intra-ligand π-π* transitions of **[Ru(C2)$_2$(NCS)$_2$]$^{2+}$** and **[Ru(C3)$_2$(NCS)$_2$]$^{2+}$**, respectively [47]. Broad absorptions extending to ∼700 nm without maxima were attributed to the MLCT transitions for **[Ru(C2)$_2$(NCS)$_2$]$^{2+}$** and **[Ru(C3)$_2$(NCS)$_2$]$^{2+}$**. Because of extension of electron delocalization over the whole molecule, di-anchoring complexes **[Ru(C2)$_2$(NCS)$_2$]$^{2+}$** and **[Ru(C3)$_2$(NCS)$_2$]$^{2+}$** exhibited red-shifted absorption compared to the mono-anchoring complexes **[Ru(bpy)$_2$C2]$^{2+}$** and **[Ru(bpy)$_2$C3]$^{2+}$** [48]. The absorption spectra of the six dyes adsorbed on TiO_2 are shown in Figure 2. For comparison, absorption peak maxima were normalized to 0.4. The absorptions are

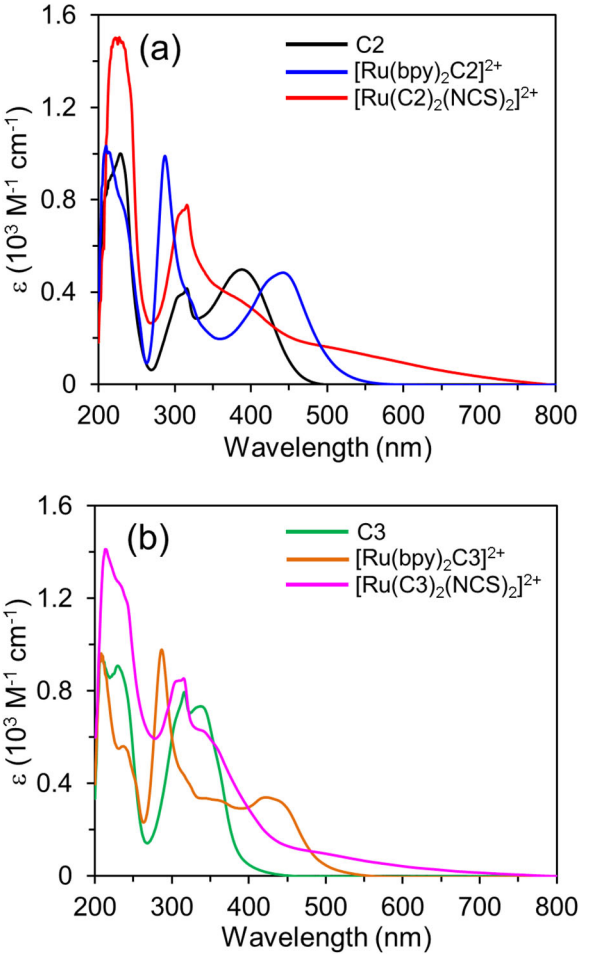

Figure 1. Absorption spectra of the catechol dyes (a) and the boronic acid dyes (b) in methanol (1×10^{-3} mol/L).

broadened and red-shifted, indicating formation of J-aggregates when compared to the corresponding solution spectra [49].

3.3. Photovoltaic performance of DSSCs

The current density – voltage (*J–V*) curves of DSSCs based on the six dyes under 100 mW cm^{-2} simulated AM 1.5 G full sunlight are demonstrated in Figure 3, and the related photovoltaic data are summarized in Table 2. As seen from Figure 3(a,b), without coadsorbent chenodeoxycholic acid (CDCA), the overall PCEs of the dyes are 0.52–2.37%, with an order of **[Ru(bpy)$_2$C3](PF$_6$)$_2$** < **C3** < **[Ru(C3)$_2$(NCS)$_2$](PF$_6$)$_2$** < **[Ru(bpy)$_2$C2](PF$_6$)$_2$** < **C2** < **[Ru(C2)$_2$(NCS)$_2$](PF$_6$)$_2$**. As seen in Table 2, the catechol dyes (**C2** and its complexes) possessed significantly higher dye loading than those of the boronic acid dyes (**C3** and its complexes), indicating that the former anchoring group has stronger binding on the TiO_2 surface compared to the latter, resulting in higher PCE values of 1.85% (**C2**), 1.67% (**[Ru(bpy)$_2$C2](PF$_6$)$_2$** and 2.37%

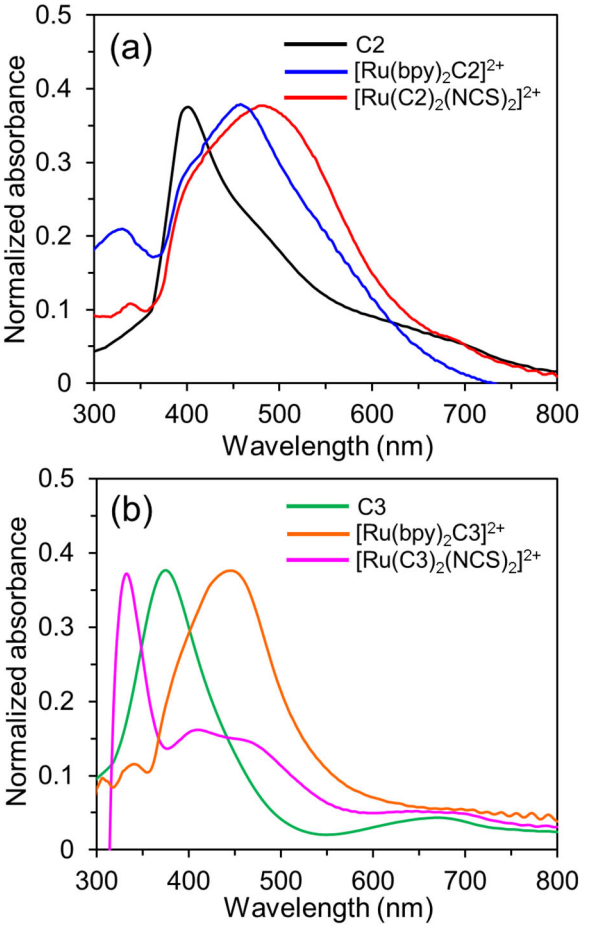

Figure 2. Absorption spectra of the catechol dyes (a) and the boronic acid dyes (b) on TiO_2 film.

Table 1. Optical properties of the dyes.

Dye	λ_{max} [nm][a] (ε [$\times 10^3$ M^{-1} cm^{-1}][a])	λ_{onset} [nm][a]	$\lambda_{max}(TiO_2)$[nm][b]	$E_{0\text{-}0}$ [eV][c]
C2	228 (1.00), 316 (0.42), 388 (0.50)	466	398	2.66
$[Ru(bpy)_2C2]^{2+}$	210 (1.03), 287 (0.99), 442 (0.48)	515	458	2.41
$[Ru(C2)_2(NCS)_2]^{2+}$	227 (1.50), 316 (0.78), 386 (0.36)	461	482	2.69
C3	229 (0.91), 316 (0.80), 337 (0.73)	397	367	3.12
$[Ru(bpy)_2C3]^{2+}$	208 (0.96), 287 (0.98), 423 (0.34)	498	444	2.49
$[Ru(C3)_2(NCS)_2]^{2+}$	214 (1.41), 315 (0.85), 353 (0.58)	436	466	2.84

[a]λ_{max}: absorption maximum wavelength; ε: molar extinction coefficient; λ_{onset}: absorption onset wavelength.
[b]$\lambda_{max}(TiO_2)$: absorption maximum wavelength on the TiO_2 film.
[c] E_{0-0}: band gap, calculated using equation $E_{0-0} = 1240/\lambda_{onset}$.

(**$[Ru(C2)_2(NCS)_2](PF_6)_2$**. The immersion time for catechol dyes being shorter than the boronic acid dyes also indicates stronger adsorption ability of the catechol moiety (see Supplementary Information). Compared with our previous dafH ligand bearing mono-hydroxylic anchoring group (**C4**) [32], using the catechol anchoring group (**C2**) proved to promote the PCE resulting from the more effective binding of the catechol on the

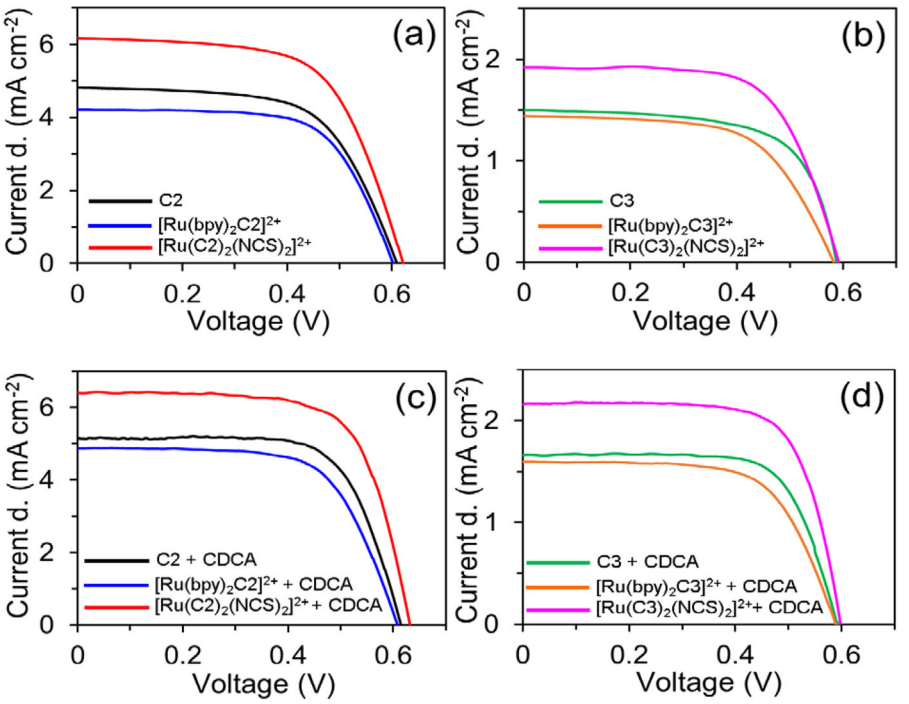

Figure 3. *J-V* curves of DSSCs based on the six dyes in the absence (a and c) and presence of chenodeoxycholic acid (CDCA) (b and d).

Table 2. Photovoltaic parameters of the dye-sensitized solar cells (DSSCs) with and without chenodeoxycholic acid (CDCA).

Dye	J_{sc}^{IPCE} (mA cm^{-2})[a]	J_{SC} (mA cm^{-2})	V_{OC} (V)	FF	PCE (%)	Dye loading amount (mol cm^{-2})
C2	4.68	4.82	0.609	0.63	1.85	3.51×10^{-7}
C2 + CDCA		5.15	0.614	0.69	2.18	3.25×10^{-7}
[Ru(bpy)$_2$C2](PF$_6$)$_2$	4.27	4.20	0.602	0.66	1.67	1.24×10^{-7}
[Ru(bpy)$_2$C2](PF$_6$)$_2$ + CDCA		4.88	0.608	0.67	1.99	1.01×10^{-7}
[Ru(C2)$_2$(NCS)$_2$](PF$_6$)$_2$	6.24	6.16	0.621	0.62	2.37	2.37×10^{-7}
[Ru(C2)$_2$(NCS)$_2$](PF$_6$)$_2$ + CDCA		6.40	0.632	0.70	2.83	2.03×10^{-7}
C3	1.43	1.50	0.587	0.67	0.59	9.01×10^{-8}
C3 + CDCA		1.66	0.593	0.71	0.70	8.71×10^{-8}
[Ru(bpy)$_2$C3](PF$_6$)$_2$	1.34	1.44	0.582	0.62	0.52	5.15×10^{-8}
[Ru(bpy)$_2$C3](PF$_6$)$_2$ + CDCA		1.60	0.589	0.68	0.64	4.86×10^{-8}
[Ru(C3)$_2$(NCS)$_2$](PF$_6$)$_2$	1.88	1.92	0.591	0.66	0.75	7.95×10^{-8}
[Ru(C3)$_2$(NCS)$_2$](PF$_6$)$_2$ + CDCA		2.16	0.598	0.72	0.93	7.59×10^{-8}
N719 + CDCA		14.8	0.770	0.68	7.75	–

[a] J_{sc}^{IPCE} values were integrated from their IPCE spectra.

TiO_2 surface [50]. When compared with the DSSCs based on mono-anchoring complexes **[Ru(bpy)$_2$C2](PF$_6$)$_2$** and **[Ru(bpy)$_2$C3](PF$_6$)$_2$**, the devices based on **C2** and **C3** show slightly higher PCE, J_{sc} and V_{oc} values due to the low dye loading of the former on TiO_2 surface [51]. The low dye loading amounts can be explained with the large sizes of **[Ru(bpy)$_2$C2](PF$_6$)$_2$** and **[Ru(bpy)$_2$C3](PF$_6$)$_2$**. Low dye loading may increase charge recombination via the uncovered TiO_2 surface, leading to the V_{oc} decrease. Additionally, the increased charge recombination may reduce the J_{sc} [50]. Among the

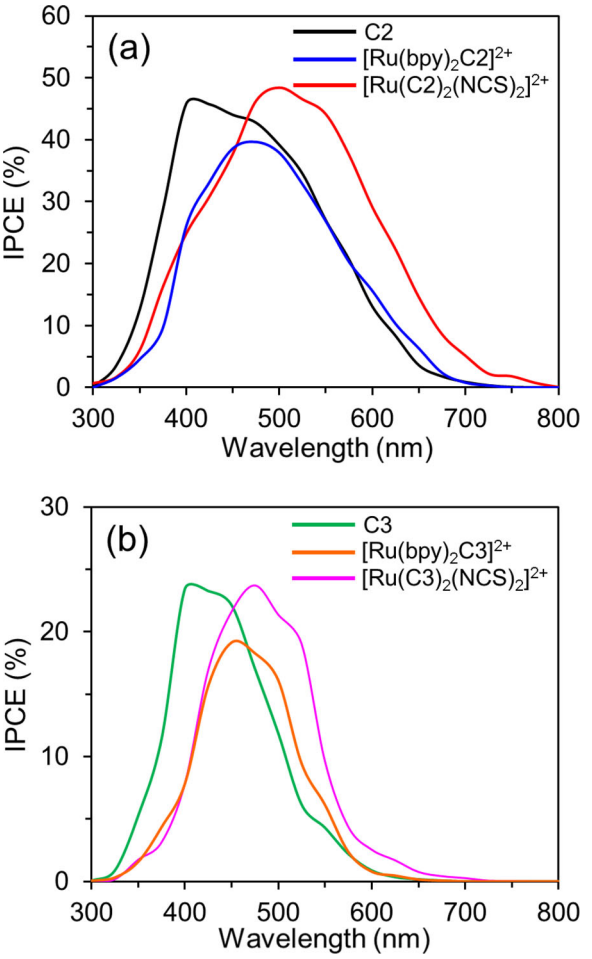

Figure 4. IPCE curves of DSSCs based on the catechol dyes (a) and the boronic acid dyes (b).

six dyes, DSSC based on the complex bearing two catechol anchoring groups (**[Ru(C2)$_2$(NCS)$_2$](PF$_6$)$_2$**) showed a maximum PCE of 2.37% (J_{sc} = 6.16 mA cm^{-2}, V_{oc} = 0.621 mV, FF = 0.62). The higher PCE of **[Ru(C2)$_2$(NCS)$_2$](PF$_6$)$_2$** is attributed to its broader absorption spectrum on the TiO_2 film [48] and appropriate dye loading [51], leading to the improvement of J_{sc} and V_{oc}, respectively. Except for **C2**, the dye loading amount of **[Ru(C2)$_2$(NCS)$_2$](PF$_6$)$_2$** is higher than those of others. Despite dye loading of **[Ru(C2)$_2$(NCS)$_2$](PF$_6$)$_2$** being lower than **C2**, DSSC based on the former exhibited higher V_{oc}. The di-anchoring dye might occupy more adsorption sites on the TiO_2 surface over a wider region than the mono-anchoring dye, which is beneficial to reduce charge recombination [52]. Moreover, the presence of two anchoring groups strengthens the binding of dye and enhances the electron injection from the dye to TiO_2 compared to the mono-anchoring group dyes [52–54].

As known, the use of CDCA with dye sensitizers can prevent dye aggregation and retard charge recombination, which is beneficial to improve the performance of DSSCs [55, 56]. On this basis, CDCA was employed for fabrication of DSSCs. In the presence of CDCA, the J_{sc}, V_{oc} and FF of DSSCs based on the six dyes are 1.60–6.40 mA cm^{-2},

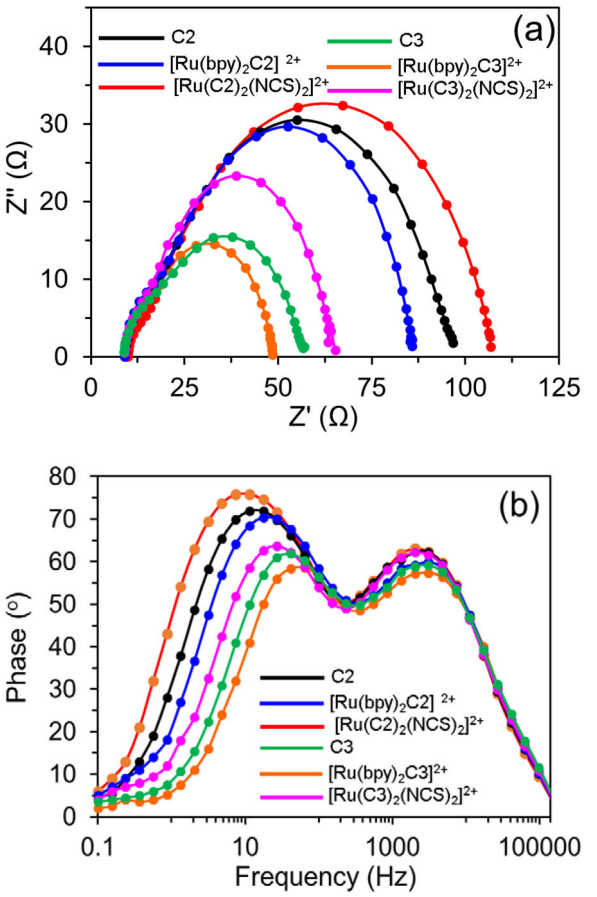

Figure 5. Nyquist (a) and Bode (b) plots of DSSCs based on the six dyes.

0.589–0.632 V and 0.67–0.72, respectively, corresponding to an overall PCE of 0.64–2.83% (Figure 3(c,d); Table 2). For comparison, the DSSC based on **N719** with CDCA exhibited a PCE of 7.75%. After addition of CDCA, only a slight increment in V_{oc} was observed for all the cells. This can be ascribed to relatively low concentration of CDCA (5 mM). All six cells exhibit over 17% PCE improvement compared with the DSSCs without CDCA, indicating that the coadsorbent decreases the aggregation and suppresses charge recombination [57]. As expected, the best PCE of 2.83% was obtained with **$[Ru(C2)_2(NCS)_2](PF_6)_2$** sensitized cell, possessing a typical J_{sc} of 6.40 mA cm^{-2}, a V_{oc} of 0.632 V, and a *FF* of 0.70.

To confirm the difference between the J_{sc} values of these dyes, the incident photon-to-current conversion efficiencies (IPCE) as a function of incident wavelength for the DSSCs were measured (Figure 4). The integrated photocurrent (J_{sc}^{IPCE}) values from the IPCE spectra are in agreement with the measured J_{sc} values (Table 2). The maxima of the IPCE peak of the catechol dyes reach 45% contrasting with the peak values of the boronic acid dyes of only ~25%. Moreover, the catechol dyes show much broader IPCE curves than those of the boronic acid dyes, which is consistent with the absorption spectra on the TiO_2 film. Therefore, the higher IPCE values and broader IPCE

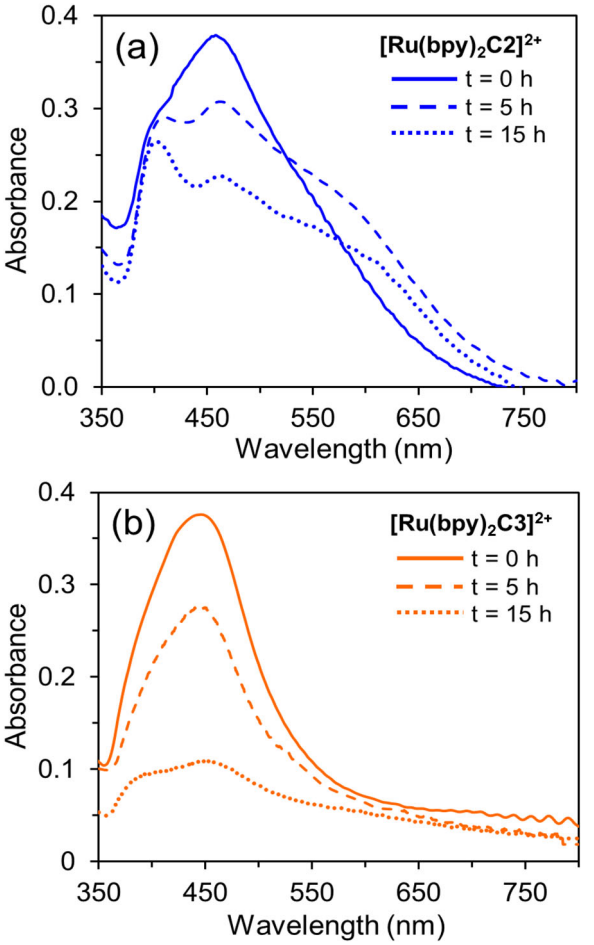

Figure 6. Absorption spectra of $[Ru(bpy)_2C2]^{2+}$ (a) and $[Ru(bpy)_2C3]^{2+}$ (b) sensitized TiO_2 films before (t = 0 h) and after 5 and 15 h of desorbing treatment.

responses of the catechol dyes confirmed their higher J_{sc} values from the *J–V* measurement [58].

To investigate the high V_{oc} observed for the catechol dyes, electrochemical impedance spectroscopy (EIS) measurements of the DSSCs were obtained in the dark. Nyquist plots of DSSCs based on the six dyes are exhibited in Figure 5(a). The larger semicircle at the lower frequencies is related to the charge recombination resistance (R_{rec}) at the TiO_2/dye/electrolyte interface. Larger R_{rec} reflects the lower charge recombination and higher photovoltage [59]. The R_{rec} values of six dyes increase in the order of $\mathbf{[Ru(bpy)_2C3]^{2+}}$ (29.6 Ω) < **C3** (33.0 Ω) < $\mathbf{[Ru(C3)_2(NCS)_2]^{2+}}$ (39.8 Ω) < $\mathbf{[Ru(bpy)_2C2]^{2+}}$ (68.3 Ω) < **C2** (82.2 Ω) < $\mathbf{[Ru(C2)_2(NCS)_2]^{2+}}$ (95.6 Ω), corresponding to the order V_{oc} values, $\mathbf{[Ru(bpy)_2C3]^{2+}}$ (0.582 V) < **C3** (0.587 V) < $\mathbf{[Ru(C3)_2(NCS)_2]^{2+}}$ (0.591 V) < $[Ru(bpy)_2C2]^{2+}$ (0.602 V) < **C2** (0.609 V) < $\mathbf{[Ru(C2)_2(NCS)_2]^{2+}}$ (0.621 V). This result implies that the DSSCs based on the catechol dyes can suppress charge recombination most efficiently, leading to higher V_{oc} values. The electron lifetimes (τ_e), which can be estimated using the equation $\tau_e = 1/2\pi f$ [60], are 2.48, 3.81, 5.87, 9.03, 13.89 and 21.37 ms for $\mathbf{[Ru(bpy)_2C3]^{2+}}$, **C3**, $\mathbf{[Ru(C3)_2(NCS)_2]^{2+}}$, $[Ru(bpy)_2C2]^{2+}$, **C2**

and **[Ru(C2)$_2$(NCS)$_2$]$^{2+}$**, respectively, which are also in agreement with V_{OC} values (Figure 5(b)).

Even small quantities of water in the redox electrolyte decrease the stability of the DSSCs since it accelerates dye desorption [61]. This was examined by immersing the sensitized TiO_2 films into an acetonitrile solution containing 5%w of water. Then, the anchoring stability of the dyes was evaluated by measuring their absorptions at different times of desorbing treatment, as shown in Figure 6. Remarkably, **[Ru(bpy)$_2$C3](PF$_6$)$_2$** sensitized TiO_2 film exhibited a notable drop in the absorbance compared to that of **[Ru(bpy)$_2$C2](PF$_6$)$_2$**. Similar behaviors were also observed for other boronic acid and catechol dyes, suggesting that the anchoring stabilities of the latter dyes are better than those of the former ones.

4. Conclusion

In this study, 4,5-diazafluorene ligands and their ruthenium(II) complexes were synthesized and characterized using ^{1}H NMR, ^{13}C NMR, FT-IR, UV-vis and mass spectroscopic methods. Their optical and photovoltaic properties were investigated. DSSCs based on the ligands displayed slightly higher photovoltaic performances compared to cells based on their mono-anchoring complexes owing to their more compact packing on the TiO_2 surface, which is beneficial to reduce charge recombination. Among the synthesized compounds, the DSSC based on the complex bearing two catechol anchoring groups (**[Ru(C2)$_2$(NCS)$_2$](PF$_6$)$_2$**) exhibited a higher PCE of 2.83% under standard conditions from enhanced J_{sc} and improved V_{oc}. It can be attributed to the strong binding ability of the anchoring groups on TiO_2. The results indicate that two catechol substituents can be incorporated into the sensitizer as anchoring groups to improve photovoltaic performance.

Disclosure statement

The authors declare that they have no conflict of interest.

Funding

This work was supported by the Scientific and Technological Research Council of Turkey (TUBITAK) Ph.D. Scholarship Program in Priority Areas (2211/C) and Council of Higher Education (YOK) Ph.D. Scholarship Program (100/2000).

References

[1] B. O'Regan, M. Grätzel. *Nature*, **353**, 737 (1991).
[2] L. Zhang, X. Yang, W. Wang, G.G. Gurzadyan, J. Li, X. Li, J. An, Z. Yu, H. Wang, B. Cai, A. Hagfeldt, L. Sun. *ACS Energy Lett.*, **4**, 943 (2019).
[3] N.A. Karim, U. Mehmood, H.F. Zahid, T. Asif. *Sol. Energy*, **185**, 165 (2019).
[4] A. Błaszczyk. *Dyes Pigm.*, **149**, 707 (2018).
[5] S. Shalini, R. Balasundaraprabhu, T.S. Kumar, N. Prabavathy, S. Senthilarasu, S. Prasanna. *Int. J. Energy Res.*, **40**, 1303 (2016).

[6] Y. Saygili, M. Stojanovic, N. Flores-Díaz, S.M. Zakeeruddin, N. Vlachopoulos, M. Grätzel, A. Hagfeldt. *Inorganics*, **7**, 30 (2019).
[7] L. Zhang, J.M. Cole. *ACS Appl. Mater. Interfaces*, **7**, 3427 (2015).
[8] K. Kloc, J. Mlochowski, Z. Szulc. *J. Prakt. Chem.*, **319**, 959 (1977).
[9] V.T. Annibale, D. Song. *Dalton Trans.*, **45**, 32 (2016).
[10] K. Zhou, J. Liu, X. Xiong, M. Cheng, X. Hu, S. Narva, X. Zhao, Y. Wu, W. Zhang. *Eur. J. Med. Chem.*, **178**, 484 (2019).
[11] S. Jäger, L. Gude, M.-S. Arias-Pérez. *Bioorg. Chem.*, **81**, 405 (2018).
[12] E. Movahedi, A.R. Rezvani. *J. Mol. Struct.*, **1139**, 407 (2017).
[13] P. Yang, M. Ren, K. Chen, Y. Liang, Q.-F. Lü, T. Zhang. *Mater. Today Commun.*, **19**, 186 (2019).
[14] Y. Yu, L.Y. Bian, J.G. Chen, Q.H. Ma, Y.X. Li, H.F. Ling, Q.Y. Feng, L.H. Xie, M.D. Yi, W. Huang. *Adv. Sci.*, **5**, 1800747 (2018).
[15] S. Shang, P.-P. Chen, L. Wang, Y. Lv, W.-X. Li, S. Gao. *ACS Catal.*, **8**, 9936 (2018).
[16] M.F. Baran, F. Durap, M. Aydemir, A. Baysal. *Appl. Organometal. Chem.*, **30**, 1030 (2016).
[17] S. Zhou, Y. Liang, K. Chen, H. Qi, S. Zhang, Z. Chen, X. Wu, Y. Shao. *J. Appl. Polym. Sci.*, **135**, 46591 (2018).
[18] S. Ghosh, A.S. Alghunaim, M.H. Al-Mashhadani, M.P. Krompiec, M. Hallett, I.F. Perepichka. *J. Mater. Chem. C.*, **6**, 3762 (2018).
[19] H. Li, J. Wang, S. Zhang, C. Gong, F. Wang. *RSC Adv.*, **8**, 31889 (2018).
[20] H. Li, S. Zhang, C. Gong, J. Wang, F. Wang. *J. Fluoresc.*, **26**, 1555 (2016).
[21] S.J. Zhang, H. Li, C.L. Gong, J.Z. Wang, Z.Y. Wu, F. Wang. *Synth. Met.*, **217**, 37 (2016).
[22] B. Deng, S. Zhang, C. Liu, W. Li, X. Zhang, H. Wei, C. Gong. *RSC Adv.*, **8**, 194 (2018).
[23] F. Zhang, Y. Guan, X. Chen, S. Wang, D. Liang, Y. Feng, S. Chen, S. Li, Z. Li, F. Zhang, C. Lu, G. Cao, B. Zhai. *Inorg. Chem.*, **56**, 3742 (2017).
[24] N. Li, Z. Fan, H. Zhao, Y. Quan, Q. Chen, S. Ye, S. Li, Q. Fan, W. Huang. *Dyes Pigm.*, **134**, 348 (2016).
[25] W.-K. Seok, A. Gupta, S.-J. Roh, W.-J. Lee, S.-H. Han. *Bull. Korean Chem. Soc.*, **28**, 1311 (2007).
[26] K. Ocakoglu, E. Harputlu, P. Guloglu, S. Erten-Ela. *Inorg. Chem. Commun.*, **24**, 118 (2012).
[27] K. Ocakoglu, S. Sogut, H. Sarica, P. Guloglu, S. Erten-Ela. *Synth. Met.*, **174**, 24 (2013).
[28] C. Cebeci, F.A. Kilicarslan, O. Gürbüz, Y. Fırat, M. Okutan, I. Erden. *Dyes Pigm.*, **134**, 77 (2016).
[29] I. Erden, C. Cebeci, F. Aytan Kilicarslan. *J. Coord. Chem.*, **70**, 2334 (2017).
[30] R. Sivakumar, A. Manivel, M. Meléndrez, J. Martínez-Oyanedel, M. Bunster, C. Vergara, P. Manidurai. *Polyhedron*, **87**, 135 (2015).
[31] R. Sivakumar, R. Recabarren, S. Ramkumar, A. Manivel, J. Alzate-Morales, D. Contreras, P. Manidurai. *New J. Chem.*, **41**, 5605 (2017).
[32] I. Erden, A. Hatipoglu, C. Cebeci, S. Aydogdu. *J. Mol. Struct.*, **1201**, 127202 (2020).
[33] C.R. Rice, M.D. Ward, M.K. Nazeeruddin, M. Grätzel. *New J. Chem.*, **24**, 651 (2000).
[34] T. Higashino, H. Iiyama, Y. Kurumisawa, H. Imahori. *Chemphyschem*, **20**, 2689 (2019).
[35] G. Ramakrishna, D.A. Jose, D.K. Kumar, A. Das, D.K. Palit, H.N. Ghosh. *J. Phys. Chem. B.*, **109**, 15445 (2005).
[36] A.O. Adeloye, P.A. Ajibade. *Molecules*, **19**, 12421 (2014).
[37] F. Ambrosio, N. Martsinovich, A. Troisi. *J. Phys. Chem. Lett.*, **3**, 1531 (2012).
[38] S. Altobello, C.A. Bignozzi, S. Caramori, G. Larramona, S. Quici, G. Marzanni, R. Lakhmiri. *J. Photochem. Photobiol. A. Chem*, **166**, 91 (2004).
[39] Ç. Kırbıyık, D.A. Kara, K. Kara, S. Büyükçelebi, M.Z. Yiğit, M. Can, M. Kuş. *Appl. Surf. Sci.*, **479**, 177 (2019).
[40] Ç. Kırbıyık, K. Kara, D.A. Kara, M.Z. Yiğit, B. İstanbullu, M. Can, N.S. Sariciftci, M. Scharber, M. Kuş. *Appl. Surf. Sci.*, **423**, 521 (2017).
[41] N. Tomar, A. Agrawal, V.S. Dhaka, P.K. Surolia. *Sol. Energy*, **207**, 59 (2020).
[42] K. Kloc, J. Mlochowski. *Z. Szulc. ChemInform*, **9**, (1978).
[43] B. Sullivan, D. Salmon, T.J. Meyer. *Inorg. Chem.*, **17**, 3334 (1978).

[44] M.S. Deshpande, A.S. Kumbhar. *J. Chem. Sci.*, **117**, 153 (2005).
[45] A. Garza-Ortiz, P.U. Maheswari, M. Siegler, A.L. Spek, J. Reedijk. *New J. Chem.*, **37**, 3450 (2013).
[46] M.K. Nazeeruddin, A. Kay, I. Rodicio, R. Humphry-Baker, E. Mueller, P. Liska, N. Vlachopoulos, M. Graetzel. *J. Am. Chem. Soc.*, **115**, 6382 (1993).
[47] C.Y. Chen, H.C. Lu, C.G. Wu, J.G. Chen, K.C. Ho. *Adv. Funct. Mater.*, **17**, 29 (2007).
[48] W. Lee, S.B. Yuk, J. Choi, H.J. Kim, H.W. Kim, S.H. Kim, B. Kim, M.J. Ko, J.P. Kim. *Dyes Pigm.*, **102**, 13 (2014).
[49] X.-M. Duan, H. Konami, S. Okada, H. Oikawa, H. Matsuda, H. Nakanishi. *J. Phys. Chem.*, **100**, 17780 (1996).
[50] G. Calogero, A. Sinopoli, I. Citro, G.D. Marco, V. Petrov, A.M. Diniz, A.J. Parola, F. Pina. *Photochem. Photobiol. Sci.*, **12**, 883 (2013).
[51] M.K. Fischer, S. Wenger, M. Wang, A. Mishra, S.M. Zakeeruddin, M. GräTzel, P. BäUerle, *Chem. Mater.*, **22**, 1836 (2010).
[52] G.E. Zervaki, P.A. Angaridis, E.N. Koukaras, G.D. Sharma, A.G. Coutsolelos. *Inorg. Chem. Front.*, **1**, 256 (2014).
[53] J.Y. Park, B.Y. Jang, C.H. Lee, H.J. Yun, J.H. Kim. *RSC Adv.*, **4**, 61248 (2014).
[54] D. Cao, J. Peng, Y. Hong, X. Fang, L. Wang, H. Meier. *Org. Lett.*, **13**, 1610 (2011).
[55] B.S. Arslan, B. Arkan, M. Gezgin, Y. Derin, D. Avcı, A. Tutar, M. Nebioğlu, İ. Şişman. *J. Photochem. Photobiol. A. Chem.*, **404**, 112936 (2021).
[56] V. Kumar, R. Gupta, A. Bansal. *Sol. Energy*, **196**, 589 (2020).
[57] F. Lu, S. Qi, J. Zhang, G. Yang, B. Zhang, Y. Feng. *Dyes Pigm.*, **141**, 161 (2017).
[58] W. Yang, D. Cao, H. Zhang, X. Yin, X. Liao, J. Huang, G. Wu, L. Li, Y. Hong. *Electrochim. Acta*, **283**, 1732 (2018).
[59] S.H. Kang, S.Y. Jung, Y.W. Kim, Y.K. Eom, H.K. Kim. *Dyes Pigm.*, **149**, 341 (2018).
[60] Y. Jiao, L. Mao, S. Liu, T. Tan, D. Wang, D. Cao, B. Mi, Z. Gao, W. Huang. *Dyes Pigm.*, **158**, 165 (2018).
[61] R. Grisorio, L. De Marco, G. Allegretta, R. Giannuzzi, G.P. Suranna, M. Manca, P. Mastrorilli, G. Gigli. *Dyes Pigm.*, **98**, 221(2013).